This is the peer reviewed version of Toumpanaki, E., Lees, J.M. and Terrasi, G.P. (2018) Bond Durability of Carbon Fibre Reinforced Polymer (CFRP) Tendons Embedded in High Strength Concrete, accepted for publication in *ASCE Journal of Composites for Construction*

Bond Durability of Carbon Fibre Reinforced Polymer (CFRP) Tendons Embedded in High Strength Concrete

Eleni Toumpanaki[1], Janet M. Lees[2], Giovanni P. Terrasi[3]

Abstract

The structural performance of Carbon Fibre Reinforced Polymer (CFRP) pretensioned structures is controlled by the bond between the CFRP tendons and concrete. The bond strength of CFRP sand-coated tendons can be affected by humid environments due to the porous epoxy matrix structure or by defects in the external sand coating layer of CFRP tendons e.g. due to storage conditions. Pull-out tests were carried out to assess the bond strength performance of sand-coated tendons embedded in high strength concrete and immersed in water at either 23°C or 40°C. Sand-coated CFRP tendons with two different core diameters of either 4.2 mm or 5.4 mm were studied. To assess the effect of the sand coating coverage on the bond, half sand-coated and uncoated tendons were also tested. An image processing technique was developed to help correlate bond strength variations with variations in the sand coating. An average difference of 24% between the bond strengths of the half sand-coated and full sand-coated tendons was recorded. A large scatter in the pull-out results for the sand-coated tendons of diameter 5.4 mm was observed and this was attributed to the manufacturing process. There was no clear trend of bond strength degradation in the sand-coated tendons even after roughly 1.5 years of full immersion in water irrespective of the exposure temperature. However, an increase in the bond strength of the uncoated tendons

[1] Research Associate, Centre for Natural Material Innovation, University of Cambridge, 1-5 Scroope Terrace, Cambridge, CB2 1PX, Tel: +44(0)1223760124, email: et343@cam.ac.uk (corresponding author)

[2] Professor, Department of Engineering, University of Cambridge, Trumpington Street, Cambridge, UK, CB2 1PZ, e-mail: jmL2@eng.cam.ac.uk

[3] Head, Laboratory for Mechanical Systems Engineering, Swiss Federal Laboratories for Materials Science and Technology (EMPA) and visiting Professor at the University of Edinburgh, School of Engineering, UK Überlandstrasse 129, 8600 Dübendorf, Switzerland, e-mail: giovanni.terrasi@empa.ch

and in the bond stiffness of all CFRP tendons was observed. This was felt to be the result of concrete autogenous shrinkage in high strength concrete and the potential swelling effects of the tendons in a humid concrete environment. Analytical models are used to describe the bond stress-slip behaviour and their suitability for sand coated CFRP tendons is studied.

Keywords: Carbon fiber reinforced polymer, Durability, Bond strength

Introduction

Incidents of severe corrosion in steel reinforcement and steel prestressing tendons have been reported in structural applications such as bridges (Lynch 2012), off-shore structures including wind turbines (Kurian et al. 2009) and even power stations (Guimaraes and Burgoyne 1987). These problems can be the result of a poor structural design or construction deficiencies that enable corrosive materials, such as water and deicing salts, to come into direct contact with the steel. In prestressed concrete, steel corrosion can lead to brittle catastrophic failures as demonstrated by the collapse of the West Berlin Congress Hall (Feld and Carper 1997). Prestressing tendons are usually loaded up to 70% of their ultimate tensile strength. Consequently, the additional margin that allows for an increase in steel stress due to a reduction in the effective cross-sectional area as a result of corrosion is limited.

Carbon Fibre Reinforced Polymer (CFRP) materials can be a proactive means to avoid chemical corrosion and recurrent prohibitive repair costs. CFRPs are not susceptible to corrosion, have a high strength to weight ratio and are easier to handle resulting in lower transportation and installation costs. Relative to other commonly available Fibre Reinforced Polymers (FRPs), CFRP tendons can have a higher initial cost but exhibit a greater fatigue and creep resistance, lower relaxation losses when prestressed and a superior durability in a concrete alkaline environment (Ceroni et al. 2006). Prestressed concrete allows for the tensile strain and strength capacity of CFRPs to be more fully exploited (Burgoyne and Balafas 2007), and the deflections of the structural members can remain within the

46 serviceability criteria. CFRP rods have a higher tensile strength (up to 2400MPa) than steel
47 rods that is underutilised when used in reinforced concrete. Prestraining CFRP rods in
48 concrete results in lower curvatures when both materials are designed to reach their strain
49 limits at the same time (Burgoyne 1993).
50 In pretensioned applications, the CFRP tendons are in direct contact with the concrete and
51 the prestressing load is transferred to the concrete through the bond between the CFRP
52 tendons and concrete. To increase the bond strength, sand particles can be attached to the
53 external surface of CFRP tendons. Although, uni-directional CFRP tendons exhibit very good
54 mechanical characteristics in the longitudinal-fibre direction, their stress-strain curves are
55 linear elastic up to sudden failure. The tendons are also weaker in the transverse direction
56 where the properties of the matrix material and the fiber-matrix interphase dominate. Under
57 humid conditions, the matrix tends to absorb water and consequently swells and plasticises
58 leading to a degradation of the mechanical properties (Ceroni et al. 2016). To date, design
59 guidelines for concrete reinforced with carbon FRP (CFRP) have proposed strength reduction
60 factors for environmental exposure. However, these may not reflect the complexities of the
61 stress field interactions and there can be a lack of underlying evidence to support the
62 recommendations (Huang and Aboutaha 2010). Strength reduction factors tend to relate to
63 fibre dominated properties, such as tensile strength (ACI 2006), but do not necessarily reflect
64 matrix dominated properties, such as the bond performance, shear strength, dowel strength
65 and creep, all of which can be degraded due to exposure in wet environments. Another factor
66 not explicitly considered by standards is the manufacturing process of the CFRP tendons and,
67 in particular, the curing (Krishna et al. 2010). All these factors can affect the bond strength of
68 CFRP tendons. This is important in pretensioned structures where the anchorage mechanism
69 (transfer of the prestressing force) and the structural integrity are ensured through the bond.
70 The aims of this study are to shed light on the bond durability performance of sand-coated

CFRP tendons when embedded in high strength concrete and directly exposed in water, and to study the quality of the sand coverage in CFRP tendons.

Bond performance of CFRP tendons

The bond stress transfer between FRP tendons and concrete is characterised by the combined effects of chemical adhesion, mechanical interlocking and friction. In sand-coated tendons adhesion and friction have been proposed as the main bond mechanisms (Cosenza et al. 1997) but concrete pull out failure mechanisms (Al-Mahmoud et al. 2007; Robert et al. 2009) have also been reported suggesting that high bearing stresses can develop from the mechanical interlocking effect. Friction provides the main bond resistance after bond failure takes place. The bond behaviour is affected by the concrete strength, the tendon diameter and the FRP surface profile. Depending on these factors, failure may take place within the concrete, at the concrete/FRP interface or at the outer resin/core tendon interface.

The concrete strength can affect the bond strength of CFRP rods if it is lower than a certain limit (15 MPa (Achillides and Pilakoutas 2004) or 30 MPa (Pecce et al. 2001)) such that failure takes place in the concrete. Otherwise, the failure interface resides within the resin layer. Different surface deformation patterns of the FRP rods or a lack of experimental data in certain concrete strength ranges lead to different conclusions about the proposed limit concrete strength values (15-30 MPa). A concrete strength dependency can also be reflected in the bond stress slip performance of CFRP sand-coated tendons. Baena et al. (2009) observed that in normal strength concrete (f_{cu}=27−30 MPa) the bond degradation after failure was smoother and associated with the pull out of the sand particles, whereas in higher strength concrete (f_{cu}=47−55 MPa) the bond decay was sudden followed by the shearing off of the whole sand coating and resin rich layer. Mixed-type bond failures have been also reported for concrete strengths of 25-40 MPa (Tepfers and Karlsson 1997; Lee et al. 2008). An increase in the bond strength has been observed with increasing concrete strength (Lee et

al. 2008) as a function of the ratio of the failure interface in the concrete to that in the resin. In high performance concrete, higher bond strength values compared with normal concrete have been obtained due to the beneficial confining action of the autogenous shrinkage (Larrard et al. 1993, Sayed et al. 2011).

According to Achillides and Pilakoutas (2004), FRP bars with a greater diameter develop a lower bond strength due to the synergistic effects of the Poisson's ratio effect (anisotropic behaviour of FRPs) and shear lag. Shear lag would be expected to be more pronounced in specimens with a lower Young's modulus and with a rich outer resin layer leading to a non-uniform distribution of the normal axial stresses (Figure 1a). An overview of investigations into the effect of the bar diameter on the average bond strength is depicted in Figure 1b. Tests associated with CFRPs, Glass Fibre Reinforced Polymers (GFRPs) and steel have been differentiated. Most experimental data is based on embedment lengths of 5 and 10 times the bar diameter and the average bond strength derives from the pull out load divided by the surface bonded area. A decrease in bond strength with increasing diameter was generally observed with the exception of results reported in Davalos et al. (2008). Achillides and Pilakoutas (2006) found that the difference in the Young's modulus between FRP bars (CFRP versus GFRP) seemed not to influence the shear lag effects although GFRP bars showed a greater splitting tendency in beam tests when an adequate cover was not provided. Larrard et al. (1993) carried out beam bond tests on high performance concrete specimens reinforced with deformed steel bars and a 50% decrease in the bond strength was reported with a 15 mm increase in diameter. This substantial difference was attributed to a decrease in the compressive confining stresses from the concrete autogenous shrinkage. GFRP bars embedded in high strength concrete (f_{cu}=79 MPa) (Chaallal and Benmokrane (1993)) developed a 5–23% lower bond strength when the diameter was increased by 25% whereas GFRP bars with the same difference in diameter in normal strength concrete showed a

smaller variation in bond strength (3–17%). It has been argued that the longer embedment lengths in pull-out tests with higher bar diameters result in lower average bond strengths due to the non-uniform bond stress distribution (Achillides 1998). Baena et al. (2009) highlighted that among FRP bars with the same surface profile, the deformation pattern is 'denser' in smaller diameters and bond stress-slip curves with more abrupt strength losses after failure can result. In the same study, the differences in the diameter seemed not to affect the stiffness of the bond stress-slip curves but FRP bars with a higher Young's modulus demonstrated higher bond stiffness in the ascending branch of the bond stress-slip relationship.

The FRP surface profile plays a significant role in the bond strength. Smooth CFRP rods exhibit a poor bond performance (1–3 MPa) due to the absence of the mechanical interlocking mechanism and they are mainly used for research purposes. The effect of the resin type on the adhesive bond strength in terms of chemical bonding is not fully understood and Nanni et al. (1995) showed that the composition of the outer resin rich layer plays a role. The resin rich layer can enhance the shear lag phenomena in the smooth rods leading to lower bond performances. However, bond strength values of smooth CFRP rods of up to 25 MPa have been reported in ultra high performance fibre reinforced concrete by Sayed et al. (2011) due to the confinement from autogeneous shrinkage. In sand-coated tendons the bond strength has been shown to be related to the grain size in the sand coating layer and the resulting variations in the mechanical interlocking effect. However, a direct relationship between grain size and bond strength based on previous experimental studies (Okelo and Yuan 2005; Esfandeh et al. 2009; Sayed et al. 2011) remains inconclusive. Most studies make no direct reference to the grain size of the sand particles. Moreover, the development of a variable to quantify the surface profile is difficult for sand-coated tendons due to the irregularity of the surface profile pattern.

145 Al Mahmoud et al. (2007) did a comparative analysis on the effect of the grain size
146 distribution (0.1-0.2, 0.2-0.3 and 0.3-0.4 mm) on the bond performance by testing pultruded
147 CFRP rods with a diameter of 12 mm. The greatest bond strength was reported for grain sizes
148 in the range of 0.2-0.3 mm. A refinement in the grain size changed the bond failure from full
149 shearing off the sand coating layer (sand particles and resin rich layer) to the shearing off of
150 the sand particles for grain sizes between 0.1-0.2 mm. At a given concrete strength, the bond
151 decay after failure was smoother for grain sizes of 0.1-0.2 mm. An increase in the bond
152 strength of sand-coated FRP bars with coarse grain size has also been reported elsewhere
153 (Nurchi and Matthys 2002; Guadagnini et al. 2004). However, differences in the fibre type
154 and Young's modulus should also be considered.
155 In conclusion the bond strength depends on the combined effect of the concrete strength,
156 the diameter, the surface geometry, the sand coating and the mechanical properties of the
157 external resin layer. These parameters dictate how the bearing stresses developed during the
158 pulling out of the FRP bar can be resisted by the concrete keys between sand particles of the
159 FRP bar. An increase in the sand particle size increases the area of the concrete key between
160 adjacent sand particles and a shearing off failure of the whole sand coating layer is more
161 likely. However, the bond strength of a sand-coated CFRP tendon relies not only on the
162 percentage of the sand particles but also on the stiffness and the mechanical properties of the
163 external resin layer where the bond failure interface lies. These properties can be greatly
164 affected by the curing conditions during the manufacturing process.
165 **Effect of humid environments on the bond strength of FRP bars**
166 To study the long-term bond performance of FRP bars several methods to accelerate time
167 have been adopted including exposure to high temperatures or high humidity environments.
168 The simulated conditions should be representative of the field conditions and consider the
169 effect on the interaction between concrete and CFRP reinforcement. There is no standard

method for determining the FRP–concrete bond durability but two methodologies have been proposed in the literature. The first consists of pre-exposing the CFRP reinforcement directly to wet solutions and then casting the tendon in concrete (Al-Dulaijan et al. 2001; Ward 2009; Bakis et al. 1998). The influence of the concrete as a protective layer for the tendon is neglected. However, there are concerns that the degradation induced in this way is not representative of the actual environmental conditions and is potentially too aggressive. The second method involves exposing FRP-concrete pull-out specimens to high humidity environments at elevated temperatures (Davalos et al. 2008; Porter and Barnes 1998, Robert and Benmokrane 2010; Zhou et al. 2012;). The elevated temperature accelerates time based on the Arrhenius principles. However, thermal expansion and swelling effects of the epoxy in the CFRP reinforcement should also be considered. A rise in temperature seems to be beneficial for the early concrete strength, but may have an adverse affect from about 7 days onwards (Neville 2011), due to a non-uniform distribution of the hydration products (Verbeck and Helmuth 1968) after a rapid initial curing. However, this effect should be more limited in high strength concrete with a lower water/cement (w/c) ratio (ACI 305R-91).

Past research on the bond durability of FRP bars has tended to focus on GFRP bars and polyester and vinylester matrices. The experimental findings are contradictory and there is no clear conclusion on the effect of humid conditions in the bond strength of FRP bars. An insignificant bond strength degradation of GFRP rods with a vinylester resin has been observed when pull-out test specimens were immersed in either a concrete alkaline or water bath at 60°C (Porter and Barnes 1998) or in tap water at either 23°C or 40°C or 50°C (Robert and Benmokrane 2010). In the latter study, material degradation was not observed as confirmed with optical microscopy pictures and Differential Scanning Calorimetry (DSC) tests (T_g values). However, Bank et al. (1998) observed white blistering in smooth GFRP rods with polyester or vinylester resin after exposure of concrete specimens in tap water at 80°C

for 12 weeks. They argued that the resulting surface roughening had a beneficial effect on the bond strength (mechanical interlocking). It was postulated that the immersion conditions filled the concrete pores with alkaline solution and led to the deterioration of the surface of the rods as observed from optical microscopy pictures.

Davalos et al. (2008) noted a bond strength reduction of about 7-10% for sandblasted CFRP bars and 5-20% for sand-coated GFRP bars (vinylester) after immersion in water at 23°C or 60°C for 90 days. Other helically wrapped and sand-coated GFRP products with a vinylester matrix tested in the same study showed more severe surface degradation and colour changes under the same exposure conditions. The exposure increased the slip values at the free end but there was no change in the bond failure mode. Temperature fluctuations seemed to deteriorate the adhesion bond mechanism in GFRPs and cause concrete microcracking. Ward (2009) preconditioned smooth and sand-coated CFRP tendons at 20°C and 60°C in water for up to 13 weeks. The exposed tendons were then cast in concrete and the FRP-concrete samples subsequently immersed in a water tank at 20°C. An estimated decrease of 10% was observed in sand-coated tendons preconditioned in water at 60°C compared with specimens preconditioned in water at 20°C for 1 week. Firm conclusions for the sand-coated tendons could not be drawn due to the scatter in the experimental data, possibly due to the sand coating variability. Scott (2009) observed from Scanning Electron Microscopy (SEM) pictures that exposure of CFRP tendons to concrete pore solution can lead to a slight corrosion of the sand particles. However, Robert and Benmokrane (2010) observed no degradation at the interface between sand coating layer and concrete of exposed pull-out test GFRP specimens by carrying out optical microscopy. Al-Dulaijan (2001) pre-conditioned smooth and machined glass/vinylester rods in various solutions (ammonia, acetic acid and deionised water) for 28 days and then cast them in concrete to carry out bond tests. A 115% increase in the bond strength of smooth glass/vinylester rods was observed due to

surface roughening. Smooth carbon epoxy bars in ammonia showed a 37% decrease in bond performance that was attributed to the competing mechanisms of surface roughening and matrix plasticisation. The machined rods were manufactured by lathing the surface of smooth rods and thus the protective resin rich layer was removed. The fibre/matrix interface was directly exposed and the bond strength reductions were more pronounced. Existing experimental results relating to the bond performance after exposure are summarised in Figures 2a and 2b. It can be concluded that GFRP bars, usually associated with a vinylester or polyester matrix, show an inferior bond performance compared with CFRP bars with an epoxy matrix. This is the result of observed white blistering, plasticisation and degradation of the matrix layer in most GFRP studies that can either yield lower or higher bond strength due to the enhanced mechanical interlocking effect in the latter case. Observed experimental variations among authors can be also attributed to differences in the chemical structure of the matrix component of FRP bars among manufacturers that is usually proprietary. Different matrices exhibit different long-term durability performance, whereas the continuous developments of matrix formulations by suppliers can affect the intended mechanical performance (Lees et al. 2016) and durability. Another aspect to consider is how the concrete environment including the internal moisture conditions and concrete alkalinity interacts with the FRP bars. High permeability is expected in concrete with high w/c ratios where the capillary pores are filled with water. In highly permeable concrete, FRP bars can be more susceptible to degradation due to the greater presence of concrete pore solution. However, at similar w/c ratios increases in bond performance were observed for FRPs with a polyester matrix at longer exposure times (Abbasi and Hogg 2005; Zhou et al. 2012). The effects of competing mechanisms such as swelling effects, concrete shrinkage (low w/c ratio) and matrix degradation on the bond strength of FRP tendons within a concrete environment are difficult to differentiate.

245 **Experimental programme**

246 An experimental programme was designed to investigate the bond performance of sand-
247 coated CFRP tendons cast in high strength concrete and immersed in water.

248 **Materials**

249 Three groups of CFRP tendons, C-UN, C-SL and D were tested. The material and the
250 mechanical properties of the tendons are summarised in Table 1. The group C-UN and D
251 tendons have the same carbon fibre and epoxy material. The group C-SL tendons differ in
252 their epoxy and carbon fibre type and exhibit a 5% higher elastic Young's modulus and a
253 43% higher tensile strength than group D tendons. The group D tendons have a larger
254 diameter (D=5.4 mm) than the group C-SL and C-UN tendons (D=4.2 mm).

255 The sand-coated tendons as supplied by the manufacturer were denoted as full sand-coated
256 tendons (FS). Partial losses of sand particles, unevenly distributed, were observed. This was
257 attributed to handling, storage and transportation conditions in industry. Partial sand-coated
258 tendons were manually prepared from the group C-SL by removing the sand coating layer
259 with a blade over half the surface of a typical sand-coated tendon. These specimens were
260 denoted as half sand-coated tendons (HS). The stiffest and densest sand coated region, as
261 visually identified, was preferentially selected to be retained in the half sand-coated tendons.
262 The manufacturing process of the sand coated tendons consists of two principal steps. Firstly,
263 the core tendon diameter is manufactured by pulling the carbon fibres through a resin bath.
264 The fibres are aligned into a compact cylindrical geometry and the first curing takes place in
265 the preformer dies. Secondly, the external sand coating layer is manufactured. Resin is
266 injected on the tendons from the top and spraying of the sand particles follows. A second
267 heating process occurs to cure the outer resin rich layer. Before the second curing process
268 agglomeration of resin and sand particles is postulated to take place at the bottom of the
269 tendon due to gravity. This is the reason why a stiffer sand coating layer was observed in

almost half of the surface. As will be discussed, an image processing method was developed to quantify the variations in the sand coating layers. Smooth tendons (Group C-UN) with a diameter of 4.2 mm were also tested. The surface conditions of the CFRP tendons studied are schematically shown in Figure 3a. Figures 3b and 3c show the outer layer of a sand-coated and uncoated tendon respectively. No resin rich layer was observed in the uncoated tendon profile as provided by the manufacturer.

The high performance concrete consisted of a mix of high strength cement CEM I 52.5R, fly ash, micro-silica and PP fibers. The maximum size of the aggregates used was 6 mm. Two concrete mixes I and II were cast. The differences between the mixes lie in the w/c ratio, the amount and type of plasticiser, the application of vibration and the curing process (air or wet) after casting. Concrete mix I was used for the full and half sand-coated tendons from group C-SL and for the C-UN smooth tendons. The group D sand-coated tendons were cast with concrete mix II. All these variables are summarised in Table 2. The slump flow in both concrete mixes was measured according to ASTM C1611/C1611M (ASTM 2009) standards.

Test Methods

All the pull-out test specimens consisted of a 300 mm CFRP tendon concentrically embedded in a 100×100×100 mm concrete cube. A central bonded region of 40 mm was provided for all the tendons irrespective of the diameter. This corresponded to 9.5D for groups C-UN and C-SL and 7.4D for group D where D is the diameter of the core tendon (see Table 1). Two unbonded regions at the free and loaded end were formed with plastic tubes before casting. The loaded end is defined as the end closer to the crosshead of the Instron machine where slip values are first recorded during pulling out (see Figure 4). The sand coating on the unbonded region at the free end was removed with a sharpened blade. This enabled a more representative measurement of the bond friction component by avoiding a coated region entering the failure interface and thereby artificially increasing the residual

295 bond strength. Concentric pull-out tests were adopted to measure the bond performance
296 between the CFRP tendons and concrete due to their simplicity and for reference with
297 existing literature. The pull-out tests were carried out in an Instron machine with a 30 kN
298 load cell capacity in a displacement control mode. The testing machine head speed was 0.5
299 mm/min and satisfied the ACI 440 guidelines (ACI 2001) for pull-out tests (speed not greater
300 than 1.27 mm/min). The CFRP reinforcement was pulled out from the concrete block that
301 reacted against a fixed steel plate. A layer of plaster was applied on the top concrete loaded
302 face to ensure a uniform contact with the steel plate. Details of the test set up are depicted in
303 Figure 4. The loaded end and free end slip values were recorded with Linear Variable
304 Differential Transformers (LVDTs). Any displacement of the steel reaction plate was
305 recorded with an LVDT during testing. Two strain gauges were attached to the CFRP tendons
306 at the loaded end. Mechanical wedge anchors were used to grip the full and half sand-coated
307 tendons. However, expansive cement anchors were required for the smooth uncoated
308 tendons. The loaded end of the uncoated CFRP tendon was potted in a steel tube with a
309 diameter of 38 mm, thickness 6 mm and length of 100 mm with BRISTAR expansive cement
310 using 1.9 kg/m (per unit length of tube) and a 27.5 % water content (Lees et al. (1995)). The
311 specimens were left sealed in the lab for 3 days for the expansive cement to cure.
312 The initial C-SL and C-UN tests were conducted with a different instrumentation
313 arrangement. The loaded end slip values were measured with only one LVDT and this
314 resulted in inaccuracies. Therefore, the revised test arrangement, as shown in Figure 4, was
315 adopted with 2 LVDTs attached to the loaded end of the reinforcement. To calculate the slip
316 at the loaded end, the average readings from the two LVDTs were corrected for the tendon
317 extension and plate displacement. The concrete deformation was considered to be negligible
318 and not taken into account in the loaded end slip values. Direct readings of the free end slip
319 were recorded using two LVDTs attached to the tendon.

320 **Exposure Regime**

321 To accelerate the environmental conditioning, the FRP-concrete pull-out test specimens
322 were immersed in tap water in polypropylene containers at 40°C. To avoid degradation in the
323 gripping anchorage region, the loaded end was excluded from immersion. The sealed bond
324 breakers remained in place in the immersed specimens to prevent water diffusion in the
325 CFRP/concrete interface through the ends of the bonded length. 40°C was judged to be a safe
326 accelerating temperature that would not result in concrete cracking based on an elastic thick
327 walled analysis (Aiello et al. (2001)) where the concrete cube was simulated as a cylinder
328 subjected to an internal pressure caused by the thermal expansion of the CFRP tendon.

329 The matrix of the exposure conditions for the CFRP tendons is presented in Table 3. The
330 specimens were identified as *a*-*b*-*c*-*d*-*e*, where *a* denotes the material group (C-SL, C-UN
331 with D=4.2 mm and D with D=5.4 mm), *b* denotes the concrete mix I or II, *c* denotes the
332 sand coating layer condition (FS: full sand-coated tendons, HS: half sand-coated tendons and
333 UN: uncoated tendons), *d* denotes the exposure temperature (23 or 40°C) or a control
334 specimen (c) and *e* denotes the exposure time. The curing regime for the control specimens
335 differed between concrete mixes I and II. For mix I all specimens were immersed in water at
336 23°C for 7 days and then the accelerated ageing commenced. For concrete mix II, the
337 specimens were first air cured for 14 days and then the exposure programme started with
338 immersion in water at the required temperature. In total 38 Group C specimens were tested.
339 37 Group D specimens were cast and of these 32 specimens were tested, 4 were kept for
340 future long-term testing and 1 specimen was not tested but instead used to take microscope
341 pictures to detect any potential splitting cracking from swelling and thermal effects.

342 During the scraping off of the sand coating in the unbonded regions, a stiffer coating was
343 observed in certain D-II-FS and C-SL-I-FS specimens. Higher bond strengths were expected
344 from these pull-out test specimens. Therefore, these specimens were purposely selected as a

345 control and long-term exposure specimens to detect any potential bond strength degradation
346 due to exposure and avoid any misleading conclusions. To study any bond variability in
347 adjacent regions along a CFRP tendon coil the D-II-FS CFRP tendons were cut in four
348 lengths from a continuous 1.2 m length of tendon. Two specimens from each subgroup in the
349 D-II-FS series were exposed at either 23 or 40°C and tested at the same exposure time.

350 **Image processing of sand coating layer variability**

351 To measure the variations in the sand coating layer of the full- (C-SL-I-FS and D-II-FS)
352 and half sand-coated tendons (C-SL-I-HS), microscopy photos of the bonded region were
353 taken before casting and analysed using an image processing technique. Figure 5 summarises
354 the features of the surface regions observed in the sand-coated tendons. Bare areas (Figure
355 5a), rough resin rich layers (Figure 5b), sand coated areas (Figure 5c) and agglomerated
356 regions of sand particles (Figure 5d) were identified. Figures 5e and 5f enable a better
357 visualisation of these regions in a cross-section and a bonded region of a CFRP sand coated
358 tendon respectively. The principal bond mechanism is the mechanical interlocking between
359 the concrete layer and the sand particles. A secondary mechanical interlocking mechanism is
360 generated between the concrete layer and the rough resin rich surface. The contribution of
361 this mechanism is likely to be lower since the depth of penetration of the remaining resin
362 layer in the concrete is low compared with the corresponding depth achieved through the
363 sand particles. The highest degree of mechanical interlocking is achieved through the
364 agglomeration of the sand particles. Gaps between the sand coating layer (Figure 5c) do not
365 necessarily result in a decrease in bond performance and can even enhance the mechanical
366 interlocking mechanism. The sand between consecutive gaps can act as a macro shear key
367 like the surface ribs in deformed FRP bars.

368 A Matlab script was written to process the photos for each specimen. The approach used
369 to edit the photos was based on the dilation and erosion method as described by Gonzalez et

al. (2010). This methodology is used to create areas with uniform intensity values and enhance the contrast between sand-coated, resin rich and uncoated areas. The method is summarised in Figure 6. The raw image of the bonded region Figure 6a is converted into a greyscale image Figure 6b to save computational processing time. The bond region of interest is cropped to the top half of the outlined tendon area (Figure 6c). This area was comparably brighter and enabled a better identification of the sand particles. A uniform background illumination of the uncoated area is achieved through a morphological opening technique using a "structuring element" greater than the size of a sand particle (Figure 6d & e). The bright areas of the sand particles are enhanced with a morphological closing technique and a "structuring element" small enough to suppress the dark details. An image with an enhanced contrast is then created by adding the difference of the opening from closing technique to the original greyscale image. The sand coating coverage was estimated from the intensity pixel values of the sand particle regions e.g. intensity values within the range, I=90-255, denoted a sand-coated region. The selected threshold intensity values to define the sand particle, resin rich and uncoated areas were based on average intensity values calculated from sample regions. These values were adopted as the criteria to calculate the ratio of sand particles (*Rsand*), resin layer (*Rresin*) and uncoated surface (*Run*), since each region provides a different contribution to the bond performance. The ratios were defined as the number of pixels that are within the specified range for each region divided by the total size of the cropped image. A deviation of maximum 2% was observed between images of the same coated area due to differences in light conditions. Further details can be found in Toumpanaki et al. (2014).

Bond failure mode inspection

To study the bond failure mechanism two methods were adopted. The first method, Method I, was used for the majority of the specimens and involved splitting open the pull-out

395 test specimens in the longitudinal direction (along the CFRP tendon). Further insight was
396 gained using a second method, Method II, where selected pull-out specimens were cut
397 transversely with a diamond saw. A concentric sample was cut from the specimen and cast in
398 moulds with fluorescein epoxy. The samples were placed in a vacuum for the fluorscein
399 epoxy to penetrate into the failure interface or any microcracks The fluorescein epoxy was
400 left in lab conditions to cure for 1 day. The specimens were demoulded and polished with
401 abrasive silicon paper and then studied visually in a Leica DMLM optical microscope. This
402 method was used to detect any radial cracking in the concrete layer. Optical microscopy
403 pictures were taken from slices from both the free and the loaded ends to distinguish if there
404 were any differences at the CFRP/sand coating layer interface (failed interface). The
405 unbonded length at the free end was fully immersed so any tendon swelling effects due to
406 exposure could in principle be identified from an absence of fluorescein at the interface.

407 **Experimental Results**

408 The experimental bond strengths are summarised in Table 4. The maximum bond
409 strengths, τ, were derived as the peak pull-out load divided by the surface bonded area at the
410 pultruded tendon core level, assuming an average bond stress distribution. The concrete
411 compressive strengths, the elastic modulus of the CFRP tendons back-calculated from the
412 strain readings, the slip at the loaded end at failure and the type of pull out load-slip
413 behaviour are also included in Table 4. The slip values at the loaded end obtained using the
414 initial pull-out test set up were not included because they were not comparable with the rest
415 of the data. The pull-out load-slip behaviour was classified as being either 'abrupt' or
416 'smooth' as depicted in Figure 7. The 'abrupt' load-slip plots (Figure 7a) were characterised
417 by a sudden drop after the peak load typically associated with a loud noise. In the descending
418 branch the bond strength progressively built up to a secondary peak and then gradually
419 decreased with a fairly constant gradient. The average bond strength value at the constant

420 decreasing gradient of the descending branch was taken as the frictional bond component.
421 The 'smooth' pull out load versus slip behaviour (Figure 7b) was identified by a gradual
422 decrease in pull-out load with increasing slip and no noise was noted.
423 The lowest average bond strengths, between 3.7–6.3 MPa, were recorded for the smooth
424 tendons C-UN-I-UN. This represented 17–30% of the average bond strength measured for
425 sand-coated tendons with the same diameter (C-SL-I-FS). Similar bond values for smooth
426 carbon epoxy tendons have been reported by Al-Mahmoud et al. (2007) and Nanni et al.
427 (1995). The highest bond strength values were recorded for the 4.2 mm sand-coated CFRP
428 tendons. The C-SL-I-FS average bond strength irrespective of the exposure regime was 21.0
429 ± 2.80 MPa (standard deviation-STDV). The highest standard deviations were observed in
430 the control specimens and specimens exposed at 40°C for 71 weeks where the stiffest sand
431 coating layer had been observed during the preparation of the test series. The C-SL-I-HS
432 specimens had an average bond strength value of 15.9 ± 1.10 MPa (STDV). Hence the half
433 sand-coated tendons had a 24% lower bond performance when compared with the equivalent
434 full sand-coated tendons. The average bond strength for the D-II-FS specimens, irrespective
435 of the exposure, was 9.9 ± 4.80 MPa (STDV). The D-II-FS group consistently exhibited
436 greater bond strength variations due to the sand coating variability and there was a maximum
437 absolute strength difference of 21.0 MPa between tendon lengths from the same CFRP
438 tendon coil. The pull-out load slip behaviour was mainly 'abrupt' for the full and half sand-
439 coated tendons. Analogous bond stress-slip responses have been recorded in sand-coated
440 CFRP bars with a coarse grain size in normal strength concrete (Al-Mahmoud et al. 2007;
441 Baena et al. 2009). This type of behaviour is usually related with either the shearing off of
442 the sand particles or a mixed concrete pull-out failure. In the D-II-FS series, specimens cut
443 from adjacent tendon lengths exhibited the same type of pull-out load versus slip behaviour

444 (smooth or abrupt). This emphasises the importance of the manufacturing process on the
445 bond performance in the sand-coated CFRP tendons.

446 **Discussion**

447 **Effect of tendon diameter**

448 The sand-coated tendons from group D, with a diameter D=5.4 mm, exhibited lower bond
449 strength values than the sand-coated tendons from group C-SL with D=4.2 mm. If the effect
450 of the different epoxy matrix on the bond strength is neglected, the D-II-FS specimens with a
451 28% greater diameter had on average a 53% lower bond performance than the C-SL-I-FS
452 specimens. A certain difference between the two groups of sand-coated CFRP tendons due to
453 the difference in diameter is expected due to shear lag effects. However, the difference in the
454 embedment length between the two groups should also be considered. In the C-SL-I-FS
455 specimens the embedment length ratio is 9.5D whereas in the D-II-FS specimens it is 7.4D.
456 Therefore, a more non-uniform bond stress distribution along the relatively longer
457 embedment length would imply that the relative bond strengths of the smaller diameter C-SL-
458 I-FS specimens could be even higher. A 6% drop in the bond strength of the CFRP uncoated
459 tendons with a Young's modulus E_L=158 GPa and cast in ultra high performance fibre
460 reinforced concrete was previously observed with an increase in tendon diameter of 25%
461 (Sayed et al. 2011). In the same study a decrease of 13% was recorded with an increase in
462 embedment length from 5D to 10D. The differences between the bond strengths of the C-SL-
463 I-FS and D-II-FS specimens could also be attributed to the quality of the external sand
464 coating layer, different epoxy matrix and potential differences in the manufacturing process.
465 Another factor to be considered, is the difference in the elastic modulus between group D and
466 C-SL. CFRP tendons with the same matrix (vinylester), diameter and surface profile (sand
467 coating) as GFRP tendons but higher elastic modulus have exhibited consistently higher bond
468 strength (Baena et al. 2009). However, in this study differences in the elastic modulus

469 between specimens and groups of tendons are a maximum of 5% and therefore this effect is
470 not considered to play a significant role.

471 **Bond failure mechanisms**

472 All the full and half sand-coated tendons irrespective of the exposure time and tendon
473 diameter failed at the interface between the sand coating layer and the core tendon. Figure 8a
474 shows a typical pull-out test specimen after being split open for investigation. The failure at
475 the sand coating layer interface can be seen at the loaded end where the sand coating layer of
476 the previously bonded area was full detached and adhered to the concrete. This suggests that
477 the adhesion between the sand particles and the concrete layer is high. Therefore the
478 argument that the adhesion is lost at small slip values (CEB-FIP 2000) may not be valid for
479 CFRP sand-coated tendons. In the uncoated tendons the failure interface was between the
480 CFRP outer surface and the concrete layer (see Figure 8b). A resin rich surface was not
481 observed in these tendons (Figure 3c) and therefore a potential shear failure within the matrix
482 did not occur. Using method I, mixed types of bond failure mechanisms including concrete
483 pull out and failure at the interface between the sand coating layer and the concrete were
484 observed in four D-II-FS and one C-SL-I-FS specimens. Concrete failures were mostly
485 observed at the free end of the specimens that were directly exposed in water perhaps due to
486 localised swelling effects. Microvoids were observed in most specimens at the failed sand
487 coating layer within the concrete. This could be attributed to the denser distribution of the
488 sand particles and entrapped air voids. This might also explain the mixed bond failure
489 mechanisms where failure lies in the concrete layer due to a localised weakening of the
490 cement paste. Mixed types of concrete radial splitting and failure at the interface between the
491 sand coating layer and the core tendon were mainly observed in the D-II-FS specimens
492 despite the lower bond strength developed. This mixed type of failure seems to be
493 independent of the exposure regime. However, radial cracking might have occurred in more

494 specimens but this could not be easily observed using inspection method I. Typical SEM
495 photos with bond radial cracking are depicted in Figure 9. The cracks in the uncoated tendon
496 specimens had a width of up to 2.58 μm and maximum length of 1 mm. In the sand-coated
497 tendons 2-4 diametrically opposite radial cracks were observed. The crack widths varied from
498 8-18 μm and in most cases extended to the boundary of the microscopy samples.
499 Observations of an untested D-II-FS specimen under the microscope showed no radial
500 cracking due to thermal and swelling expansion and autogenous shrinkage. Hence, the
501 cracking could be due to high bearing stresses generated during pulling out of the sand-
502 coated tendons. In the uncoated tendons, swelling effects might have a greater relative
503 influence due to their higher moisture absorption rate (Toumpanaki 2015).

504 **Effect of exposure on the maximum bond strength**

505 The average bond strengths with respect to exposure time are plotted in Figure 10. For
506 ease of comparison, time shift factors were analytically calculated for the 40°C specimens to
507 determine an equivalent exposure time at 23°C. These were based on the mass uptake rates,
508 k, from the Arrhenius relationship

$$k=A\exp(\frac{-E_\alpha}{RT}) \quad (1)$$

509 where k=mass uptake rate= $\Delta M/\Delta t$, ΔM= mass uptake, Δt= change in time, A=constant of the
510 material and moisture absorption process, E_α=activation evergy, R=universal gas constant and
511 T=Kelvin temperature, of equivalent dry uncoated CFRP tendons immersed in water at 23°C,
512 40°C and 60°C. The parameters A, E_α were derived by plotting the natural log of time to
513 reach specific mass uptake values (e.g. 0. 20% -1.60%) versus the inverse of temperature
514 ($1/T$) based on Equation 2.

$$\ln(\Delta t) = (\ln(\Delta M) - \ln(A)) + \frac{E_\alpha}{R}\frac{1}{T} \quad (2)$$

515 The time shift factor at 40°C was derived from the ratio of the mass uptake rate, k, at 40°C to
516 the mass uptake rate at the reference temperature 23°C. More details can be found in

517 Toumpanaki (2015). It was assumed that the same accelerated ageing process was activated
518 irrespective of the initial moisture content. Time shift factors of 3.1 and 3.5 were adopted for
519 the sand-coated and uncoated 40°C specimens respectively. The specimens exposed at 40°C
520 have been highlighted in Figure 10 for clarity. The error bars indicate one standard deviation
521 for specimens at each exposure time.

522 The bond strength values for the full sand-coated (C-SL-I-FS), half sand-coated (C-SL-I-
523 HS) and uncoated tendons (C-UN-I-UN) with a core tendon diameter 4.2 mm and cast in
524 concrete mix I are shown in Figure 10a at each exposure time. There was no clear trend in the
525 bond strength degradation in the group C full and half sand-coated tendons even after roughly
526 1.5 years of exposure at 40°C (220 weeks of equivalent exposure time at 23°C). An average
527 drop of 7% in bond strength was measured in the full sand-coated tendons after 71 weeks of
528 exposure at 23°C but an increase of 12% was observed for the same immersion time at 40°C.
529 A trend where the bond performance improved with exposure time was observed in the C-
530 UN-I-UN smooth tendons with a maximum increase in bond stress of 69% after roughly 56
531 weeks of equivalent exposure at 23°C. This increase can be attributed to tendon swelling and
532 concrete shrinkage although these factors seem to be less pronounced in the full sand-coated
533 tendons where the variability in the sand coating layer was a greater consideration. Similar
534 conclusions were drawn for the D-II-FS sand-coated tendons and an increase in the bond
535 performance with exposure time was observed to reach a peak of 150% after 142.6 weeks of
536 equivalent exposure as indicated in Figure 10b. Comparatively a greater scatter was observed
537 in the D-II-FS specimens.

538 **Effect of exposure on the residual bond strength**

539 The residual bond strength is defined as the friction component in the descending branch
540 of the pull-out load versus slip plots. The residual bond strength is associated with the
541 widening of the cracks and localised bond failure. This is more common in sand-coated

CFRP tendons where bond failures take place at small slip values. A high frictional bond can control the crack width and crack spacing and thus the deformability of a structural member.

The residual bond strengths of the full and half sand-coated specimens are shown as a function of exposure time in Figure 11. To calculate the residual strengths, an average of the bond stresses developed between the maximum slip at failure and a free end slip of 5 mm was calculated. The average residual bond strengths for the C-SL-I-FS, C-SL-I-HS and D-II-FS specimens irrespective of the exposure time were 7.3 ± 0.88 MPa, 7.2 ± 0.62 MPa and 5.3 ± 1.57 MPa respectively. The D-II-FS specimens showed a 27% lower residual bond strength and higher standard deviation when compared with the C-SL-I-FS specimens. This drop in residual bond strength is less than the observed 53% drop in maximum bond strength. The shear lag effects appear to be less important for the residual bond strength due to the absence of outer resin rich layer at the failed interface. The drop in residual bond strength was primarily attributed to the Poisson's ratio effect and secondarily to differences in the resin matrix. The C-SL-I-HS and C-SL-I-FS specimens had similar residual bond strengths. The residual bond strength in the C-SL group (resin/resin bond failure interface) was higher than the maximum bond strength of the uncoated tendons (concrete/CFRP bond failure interface) assuming that the difference in the epoxy material had only a small effect on the frictional component. An ascending trend was more pronounced in the D-II-FS group compared with the C-SL-I FS specimens. This could be attributed to a higher swelling expansion due to the greater diameter in the D-II-FS specimens either from the exposed unbonded free length or from the concrete humid environment, or concrete shrinkage effects.

Effect of exposure on the bond stiffness

The surrounding concrete pore solution and high concrete relative humidity conditions can have a plasticising effect on the outer resin layer that would have more of an impact on the resin fracture toughness than on the ultimate bond strength. A potential increase in toughness

567 of the sand coating layer under humid conditions can be reflected on the slip values and on
568 the gradient of the ascending branch of the bond stress-slip plots from the pull-out tests.
569 Figure 12a shows the bond stress versus relative slip (s_l-s_f, where s_l is the slip at the loaded
570 end and s_f is the free end slip) up to failure for representative specimens in the C-SL-I-FS
571 group after 8, 24 and 220 weeks of equivalent exposure time at 23°C. Higher slip values at
572 low bond stress levels were recorded for specimens tested after 8 weeks of equivalent
573 exposure. However, if the gradients of the plots are defined as the ratio of the maximum bond
574 strength to the maximum loaded end slip, there is a total overall average increase in gradient
575 of 67% between specimens exposed at 40°C for 71 weeks (220 weeks of equivalent exposure
576 at 23°C) and specimens exposed at 23°C for 8 weeks. Similar trends were observed in the D-
577 II-FS group as shown in Figure 12b with a 96% stiffer response after 46 weeks of exposure at
578 40°C (142.6 weeks of equivalent exposure at 23°C) attributed to concrete autogeneous
579 shrinkage. In Figure 12b, two typical specimens at each exposure time were plotted and the
580 plots have been truncated at 11 MPa for clarity irrespective of the higher ultimate bond
581 strength obtained by some specimens.

582 **Effect of the sand coating layer variability on the maximum bond strength**

583 To validate the image processing technique, the ratios of the sand coating layer *Rsand*,
584 resin rich layer *Rresin* and uncoated regions *Run* are plotted in Figure 13 for the group C-SL
585 half and full sand-coated tendons. The difference in the *Rsand*+*Rresin* ratio between the full
586 and half sand-coated tendons was on average 19%. This agreed well with the relevant 24%
587 average difference in the bond strength values. However, as discussed in Toumpanaki et al.
588 (2014) the identification of a clear boundary between the bare and sand coated surface in half
589 sand coated tendons was hindered by peak intensity values of remaining rough resin rich
590 surfaces that were incorrectly identified as sand particles by the programme but could also
591 play a secondary role in the mechanical interlocking effect. In the boundary region, the

592 colour of the external resin rich layer changed to a whiter surface due to the abrasion in the
593 removal of the sand particles. Figure 14 shows the bond strengths for both the C-SL-I-FS and
594 D-II-FS groups as a function of *Rsand*+*Rresin*. The trends in the *Rsand*+*Rresin* ratio
595 generally follow the trends in the bond strength variations but deviations can be observed.
596 The image processing results do not correlate well for specimens from both D-II-FS and C-
597 SL-I-FS groups where the highest bond strength values were recorded (e.g. C-SL-I-FS-c-0
598 (2) and D-II-FS-40-46 (1)). The resulting lower than expected *Rsand*+*Rresin* values were
599 attributed to the difficulty in detecting agglomerated sand particles visually observed on the
600 tendon surfaces during specimen preparation. In this case, 3D scanning of the sand coating
601 layer would be required to capture the surface morphology, since a digital image is only a 2D
602 representation of the surface. Lumps of sand particles could then be considered as a
603 corroboratory parameter in the *Rsand* value. If specimens with an agglomeration of sand
604 particles such as C-SL-I-FS-c-0 (2) and C-SL-I-FS-40-70 (1) were neglected, the difference
605 in the bond strength between full and half sand-coated tendons would drop to 21% and this is
606 closer to the theoretical value based on the imaging technique. Other parameters for
607 consideration are the chemical composition and stiffness of the sand coating layer as these
608 can vary between products and within the same batch due to differences in curing. Overall,
609 the method seems to provide a good general indication of the bond strength variations for
610 tendons within the same group, C-SL-I-FS or D-II-FS but outliers were noted.

611 **Analytical modelling of bond behaviour**

612 For design purposes several bond stress-slip models for FRP rods have been proposed in
613 the literature (Malvar 1995; Focacci et al. 2000;Cosenza et al. 1995). These analytical models
614 are either modified by established bond stress slip laws for deformed steel bars (e.g. the
615 mB.E.P. model by Cosenza et al. 1996) or recommended for FRP reinforcement and
616 prestressing applications (Bruggeling 1995). In this study we investigated the two of the most

617 commonly applied bond stress slip models for CFRP rods.

618 • **mB.E.P. model** (Cosenza et al. 1996)

619 This is a modifid version of the bond stress slip law proposed by Eligenhausen et al. (1983)
620 for deformed steel bars where the second branch of the equation is neglected

$$\tau=\tau_m\left(\frac{s}{s_m}\right)^{\alpha};s\leq s_m \quad (3)$$

$$\tau=\tau_m\left(1+p-p\frac{s}{s_m}\right);s_m<s\leq s_u \quad (4)$$

621 where α is a coefficient that describes the ascending branch, p is a coefficient that describes
622 the descending branch, τ_m is the maximum bond strength, s_m is the slip at the maximum bond
623 strength, and s_u is the ultimate slip.

624 • **C.M.R. model** (Cosenza et al. 1995)

$$\tau=\tau_m\left(1-\exp\left(-s/s_m\right)\right)^{\beta} \quad (5)$$

625 where β is a coefficient derived from the curve fitting of experimental data**.**

626 The proposed models in the literature seem not to differentiate between the different
627 variations in the external surface of FRP rods (e.g. helically wrapping, sand coating layer and
628 resin ribs). However, it should be noted that sand coated tendons usually exhibit more sudden
629 bond failures and the descending branches of the bond stress-slip plots (see Figure 7) cannot
630 be simulated by the 'softening' (more parabolic shaped) behaviour of the aforementioned
631 bond stress slip laws. To reflect the bond failure mechanism observed in the sand coated
632 CFRP tendons, the descending branch can either be simulated with a bilinear model or a
633 hyperbolic equation. In the former case the bilinear model consists of a steep gradient
634 (sudden drop) followed by a lower gradient p' that is more representative of the frictional
635 bond component. In this study a simplified unilinear bond stress slip relationship with a
636 decreasing gradient p' is proposed in lieu of Equation 4 of the mB.E.P. model for the
637 descending branch.

$$\tau=\tau_{fr}-p'(s-s_m);s_m<s\leq s_u \quad (6)$$

638 where τ_{fr} is the frictional bond strength at a value lower than τ_m

639 To define the coefficients α and β in the bond stress slip models, the maximum bond
640 strength τ_m and maximum slip s_m, several methods have been adopted in the literature. These
641 can be grouped into either analytical closed form solutions or curve fitting methods based on
642 experimental data and the assumption of a uniform bond stress distribution along the
643 embedment length. In the analytical closed form solutions, an equilibrium based or energy
644 based approach (Focacci et al. 2000) are adopted. In the former case, analytical equations are
645 derived from the equilibrium of forces between the bar, the bond stresses and the concrete
646 tensile stresses generated during pulling out of the FRP rod. In the latter, the work done by
647 the external forces is equated to the internal elastic energy of the bar (Focacci et al. 2000) or
648 in terms of the area underneath the τ-s and σ-s curves (Pecce et al. 2001).
649 Here the bond coefficients of the bond stress slip models are calculated by curve fitting the
650 experimental data. This is more accurate when small embedment lengths are used in the pull
651 out tests (*2-3D*), where a uniform bond stress distribution can be assumed along the bonded
652 length. However, with small embedment lengths, small variabilities in the surface profile can
653 be magnified and thus the bond stress-slip models can differ significantly between samples.
654 By increasing the embedment length, a lower Young's modulus of an FRP bar results in
655 greater slip values at the loaded end than at the free end. A non-uniform bond stress
656 distribution arises from the differential slip of the ends and the assumption of an average
657 uniform bond stress distribution is no longer appropriate (Pecce et al. 2001). Therefore, it is
658 possible that different bond stress-slip laws apply for the free and loaded end slip in standard
659 pull out tests with longer embedment lengths. Here emphasis is given to the loaded end slip
660 values.
661 A least squares regression analysis was adopted and applied to the experimental bond stress-
662 loaded end slip. The bond parameters and the indication of the fit R^2 for the ascending branch
663 of the mB.E.P. (Equation 3) and C.M.R. (Equation 5) bond stress-slip models and for the

linear descending branch (Equation 6) are summarised in Table 5 for full and half sand-coated tendons and uncoated tendons after 8 weeks of exposure. For the sand coated tendons values after 0, 10, 46 and 71 weeks of exposure are also listed to study differences due to exposure.

The ascending branch of the mB.E.P. model gave the best fit for all the CFRP specimens irrespective of the surface deformation and the exposure regime (see Figure 15). The linear descending bond stess slip model seems to fit well with the frictional bond experimental data, whereas the τ_{fr} coefficients are higher than the average experimental residual bond strength of the CFRP tendons. A linear ascending bond stress-slip model (α=1) seems to correlate better with the C-SL and C-UN bond stress-slip experimental curves. The different conditions in the C-SL-I-FS, C-SL-I-HS and C-UN-I-UN tendons seem not to affect the bond stiffness (exponent terms) of the respective bond stress slip laws for the same exposure time. The group D tendons with the larger diameter (D=5.4 mm) seem to yield lower exponent terms than those for group C-SL and C-UN. The average bond parameter α in the mB.E.P. model generally decreases with exposure time. A decrease in the bond parameter α results in an increase in the bond stiffness and this correlates with the experimental data. Bond coefficients α=0.178 ± 0.039 (STDV) and β=0.392 ± 0.226 (STDV) for the mB.E.P. and C.M.R. model respectively have been reported by Baena et al. (2009) for helically wrapped sand coated GFRP bars with τ_m=17.34 ± 2.67 (STDV) MPa and s_m=2.62 ± 2.28 (STDV) mm. In the same study it was highlighted that the bond parameters should be corrected for the effect of the diameter to achieve better pull out load-slip predictions. Pecce et al. (2001) adopted the mB.E.P. model and used an energy based closed form solution for deformed GFRP bars yielding α=0.245 ± 0.619 (STDV), τ_m=14.65 ± 0.11 (STDV) MPa and s_m=0.253 ± 0.181 (STDV) mm irrespective of the bonded length. Deviations on the calculated bond coefficients were also observed for the same bonded lengths.

Conclusions

The experimental findings suggest that exposure in water, irrespective of the exposure temperature (23 or 40°C), did not degrade the ultimate bond shear strength of CFRP tendons in high strength concrete. The variability in the sand coating layer seemed to greatly affect the bond strength of CFRP tendons highlighting the need for better qualitative tests during manufacturing and installation. Group C-SL sand-coated tendons with smaller diameters (D=4.2 mm) achieved approximately twice the bond strength of the group D-II-FS (D=5.4 mm) tendons. This was attributed to differences in the resins and curing and the relative influences of Poisson's ratio and shear lag effects due to the diameter differences. Half sand-coated tendons exhibited an 24% lower bond strength than full sand-coated tendons. This could provide the basis for design guidance to account for handling losses in CFRP sand-coated tendons. An image processing technique was designed to quantify the effect of the sand coating layer variations on the bond strength performance. The technique predicted the bond strength trends fairly well but as it was based on a representation of a 2D tendon profile, agglomerated sand particles that contributed to high bond strength performances could not be detected. The bond strength of uncoated smooth tendons generally increased with exposure time (up to 69%) and was potentially due to the combined effects of CFRP tendon swelling and concrete autogeneous shrinkage. An increase in the bond stiffness of the CFRP tendons was observed with increasing immersion time. An abrupt bond failure was common in the sand-coated CFRP tendons with a shearing off of the external sand coating layer. Radial cracking was also noted and attributed to the high bearing stresses in several sand-coated specimens and a higher propensity for swelling in the uncoated tendons. The mB.E.P. bond stress-slip model seems to fit better than the C.M.R. model with the experimental data of the sand coated tendons irrespective of any variations in the surface profile or in the diameter. A linear descending bond stress-slip relationship was proposed for the frictional bond

component of the sand coated tendons and seems to correlate well with the experimental results.

Acknowledgements

We are grateful to SACAC Ltd for their technical and financial support. The financial support from the Onassis Foundation (ET) is also greatly appreciated. We would also like to thank CEMEX and BASF for donating materials.

References

Abbasi, A., and Hogg, P.J. (2005). "Temperature effects on glass fibre rebar: modulus, strength and interfacial bond strength with concrete." *Composites: Part B*, 36(5), 394-404.

Achillides, Z. (1998). "Bond behaviour of FRP bars in concrete." PhD thesis. University of Sheffield.

Achillides, Z., and Pilakoutas, K. (2004). "Bond behavior of fiber reinforced polymer bars under direct pullout conditions." *J. Compos. for Constr.*, 8(2), 173–181.

Achillides, Z., and Pilakoutas, K. (2006). "FE modelling of bond interaction of FRP bars to concrete." *Structural Concrete*, 7(1), 7-16.

ACI 305R-91 (1991). "Hot weather concreting." American Concrete Institute, Farmington Hills, MI, USA.

ACI 440.1-R06 (2006). "Guide for the design and construction of concrete reinforced with FRP bars." American Concrete Institute, Farmington Hills, MI, USA.

ACI 440 (2001). "Recommended test methods for FRP rods and sheets." American Concrete Institute, Farmington Hills, MI, USA.

Aiello, M.A., Focacci, F., and Nanni, A. (2001). "Effects of thermal loads on concrete cover of fiber-reinforced polymer reinforced elements: theoretical and experimental analysis." *ACI Mater. J.*, 98(4), 332–339.

738 Al-Mahmoud, F., Castel, A., Francois, R., and Tourneur, C. (2007). "Effect of surface pre-
739 conditioning on bond of carbon fibre reinforced polymer rods to concrete." *Cement Concrete*
740 *Comp.*, 29(9), 677–689.
741 Al-Dulaijan, S.U., Al-Zahrani, M.M, Nanni, A., and Boothby, T.E. (2001). "Effect of
742 environmental pre-conditioning on bond of FRP reinforcement to concrete." *J. Reinf. Plast.*
743 *Comp.*, 20(10), 881-900.
744 ASTM (2009). "Standard test method for slump flow of self-consolidating concrete." ASTM
745 C1611/C1611M-09b, West Conshohocken, PA.
746 Bakis, C.E., Freimanis, A.J., and Gremel, D. (1998). "Effect of resin material on bond and tensile
747 properties of unconditoned and conditioned FRP reinforcement rods." *Proc., CDCC-*
748 *International conference*, B. Benmokrane ed., Sherbrooke, 525-536.
749 Baena, M., Torres, L., Turon, A., and Barris, C. (2009). "Experimental study of bond behaviour
750 between concrete and FRP bars using pull out test." *Composites: Part B*, 40(8), 784-797.
751 Bank, L.C., Puterman, M., and Katz, A. (1998). "The effect of material degradation on bond
752 properties of fiber reinforced plastic reinforcing bars in concrete." *ACI Mater. J.*, 95(3), 232-
753 243.
754 Burgoyne, C.J. (1993). "Should FRP be bonded to Conrete?." *Proc., Int. Symp. on Fibre*
755 *Reinforced Plastic Reinforcement for Concrete Structures (ACI SP-138)*, A. Nanni and C.W.
756 Dolan eds., Vancouver, Canada, 367-380.
757 Burgoyne, C.J, and Balafas, I. (2007). Why is FRP not a financial success?" *Proc., 8th Int.*
758 *Symp. on FRPs for Reinforced Concrete Structures (FRPRCS-8)*, T. Triantafillou ed.,
759 University of Patras, Greece, 1-10.
760 Bruggeling, A.S.G. (1995). 'Description of the SSR Method for the experimental
761 determination of the actual transmission length and relevant parameters.' *Technical Report*
762 *150502*, CUR, Gouda, The Netherlands.

763 CEB-FIP (2000). “Bond of reinforcement in concrete.” Comité Euro-International du Beton,
764 Lausanne, Switzerland.
765 Ceroni, F., Cosenza, E., Gaetano, M., and Pecce, M. (2006). “Durability issues of FRP rebars
766 in reinforced concrete members.” *Cement Concrete Comp.*, 28(10), 857-868.
767 Chaallal, O., and Benmokrane, B. (1993). “Pullout and bond of glass-fibre rods embedded in
768 concrete and cement grout.” *Mater Struct*, 26(3), 167–175.
769 Cosenza, E., Manfredi, G., and Realfonzo, R. (1995). ‘Analytical modelling of bond between
770 FRP reinforcing bars and concrete.’ *Proc., 2nd Int. Symp. on Non-Metallic (FRP) Reinforcement*
771 *for Concrete Structures (FRPRCS-2)*, L. Taerwe ed., Ghent, 164-171.
772 Cosenza, E., Manfredi, G., and Realfonzo, R. (1996). ‘Bond characteristics and anchorage length
773 of FRP rebars.’ *Proc., 2nd Int. Conf. on Advanced Composite Materials in Bridge Structures*, M.
774 El-Badry ed., Monreal, 909-916.
775 Cosenza, E., Manfredi, G., and Realfonzo, R. (1997). “Behavior and modeling of bond of
776 FRP rebars to concrete.” *J. Compos. for Constr.*, 1(2), 40–51.
777 Davalos, J.F, Chen, Y., and Ray, I. (2008). “Effect of FRP bar degradation on interface bond
778 with high strength concrete.” *Cement Concrete Comp.*, 30(8), 722-730.
779 Eligehausen, R., Popov, E. and Bertero, V.V. (1983). “Local bond stress-slip relationships of
780 deformed bars under generalized excitations. ” *Rep. No 83/23*, University of California,
781 Berkeley.
782 Esfandeh, M., Sabet, A.R., Rezadoust, A.M., and Alavi, M.B. (2009). “Bond performance of
783 FRP rebars with various surface deformations in reinforced concrete.” *Polym. Composite*,
784 30(5), 576–582.
785 Feld, J., and Carper, K. (1997). *Construction Failure*, John Wiley & Sons, New York.
786 Gonzalez, R.C., Woods, R.E., and Eddins, S.L. (2010). *Digital Image Processing Using*
787 *MATLAB, McGraw Hill Education, New Delhi, 440-488.*

788 Focacci, F., Nanni, A., and Bakis, C.E. (2000). 'Local bond-slip relationship for FRP
789 reinforcement in concrete.' *Journal of Composites for Construction ,* 4 (1), 24-31.
790 Guadagnini, M., Pilakoutas, K., Waldron, P., and Achillides, Z. (2004). "Tests for evaluation
791 of bond properties of FRP bars in concrete." *Proc., 2nd Int. Conf. on FRP Composites in*
792 *Civil Engineering (CICE 2004)*, R. Seracino ed., 343-350.
793 Guimaraes, G.B., and Burgoyne, C.J. (1987). "Repair of concrete bridges using parafil
794 ropes." *Proc., U.S European Workshop on Rehabilitation of Bridges*, Paris, 1-6.
795 Huang, J., and Aboutaha, R. (2010). "Environmental reduction factors for GFRP bars used as
796 concrete reinforcement: New Scientific Approach." *J. Compos. for Constr.*, 14(5), 479-486.
797 Katz, A. (2000). "Bond to concrete of FRP Rebars after Cyclic loading." *J. Compos. for*
798 *Constr.*, 4(3), 137-144.
799 Krishna, R., Revathi, A., Srihari, S., and Rao, R. (2010). "Post-curing effects on hygrothermal
800 behavior of RT-cured glass/epoxy composites." *J Reinf Plast Comp*, 29(3), 325-330.
801 Kurian, V.J., Narayanan, S.P., and Ganapathy, C. (2009). "Towers for Offshore Wind
802 Turbines." *Proc., 10th Asian Int. Conf. on Fluid Machinery (AICFM 2009)*, 475-487.
803 Larrard, F., Schaller, I., and Fuchs, J. (1993). "Effect of bar diameter on the bond strength of
804 passive reinforcement in high-performance concrete." *ACI Mater. J.*, 90(4), 333–339.
805 Lee, J.Y., Kim, T.Y., Kim, T.J., Yi, C.K., Park, J.S., You, Y.C., and Park, Y.H. (2008).
806 "Interfacial bond strength of glass fiber reinforced polymer bars in high strength concrete."
807 *Composites: Part B*, 39(2), 258-270.
808 Lees, J.M., Gruffydd-Jones, B., and Burgoyne, C.J. (1995). "Expansive cement couplers-A
809 means of pre-tensioning fibre reinforced plastic tendons." *Constr. Build. Mat.*, 9(6), 413-423.
810 Lees, J.M., Toumpanaki, E., Barbezat, M. and Terrasi, G.P. (2017). "Mechanical and
811 Durability Screening Test Methods for Cylindrical CFRP Prestressing Tendons" *J. Compos.*
812 *for Constr.,* 21(2).

813 Lynch, D. (2012). “Hammersmith flyover: returning to full strength.” *New Civil Engineer*, 98,
814 14-16.
815 Malvar, L.J. (1995). ‘Tensile and bond properties of GFRP reinforcing bars.’ *ACI Materials*
816 *Journal*, 92(3), 276–285.
817 Nanni, A., Al-Zahrani, M.M., Al-Dulaijan, S.U., Bakis, C.E., and Boothby, R.E. (1995).
818 “Bond of FRP reinforcement to concrete-experimental results.” *Proc., 2nd Int. Symp. on Non-*
819 *Metallic FRP Reinforcement for Concrete Structures (FRPRCS-2),* L. Taerwe ed., 135-145.
820 Neville, A.M. (2011). *Properties of concrete*. 5th Edition. Pearson Education Limited.
821 Nurchi, A., and Matthys, S. (2002). “Pull out tests on FRP bars in concrete.” *Proc., Int. Symp.*
822 *on Bond in Concrete from Research to Standards,* G.L. Balázs, P.J.M. Bartos, J. Cairns and
823 A. Borosnyói eds., Budapest University of Technology and Economics, Hungary, 708-715.
824 Okelo, R., and Yuan, R.L. (2005). “Bond strength of fiber reinforced polymer rebars in
825 normal strength concrete.” *J. Compos. for Constr.*, 9(3), 203–213.
826 Pecce, M., Manfredi, G., Realfonzo, R., and Cosenza, E. (2001). “Experimental and
827 analytical evaluation of bond properties of GFRP bars.” *J. Mater. Civil Eng.*, 13(4), 282–290.
828 Porter, M.L., and Barnes, B.A. (1998). “Accelerated aging degradation of glass fiber
829 composites.” *Proc., 2nd Int. Conf. on Composites in Infrastructure (ICCI’98)*, H.
830 Saadatmanesh and M. R. Ehsani eds., Tucson, 446–459.
831 Robert, M., Cousin, P., and Benmokrane, B. (2009). “Durability of GFRP reinforcing bars
832 embedded in moist concrete.” *J. Compos. for Constr.*, 13(2), 66–73.
833 Robert, M., and Benmokrane, B. (2010). “Effect of aging on bond of GFRP bars embedded in
834 concrete.” *Cement Concrete Comp.*, 32(6), 461–467.
835 Rossetti, V.A., Galeota, D., and Giammatteo, M.M. (1995). “Local bond stress-slip
836 relationships of glass fibre reinforced plastic bars embedded in concrete.” *Mater. Struct.*,
837 28(180), 340-344.

838 Sayed, A.F., Foret, G., and Le Roy, R. (2011). "Bond between carbon fibre-reinforced
839 polymer (CFRP) bars and ultra high performance fibre reinforced concrete (UHPFRC):
840 Experimental study." *Constr. Build. Mat.*, 25(2), 479–485.
841 Scott, P. (2009). "Aspects of CFRP Prestressed Concrete Durability in the Marine
842 Environment." PhD thesis, University of Cambridge, UK.
843 Tepfers, R., and Karlsson, M. (1997). "Pull out and tensile reinforcement splice tests using
844 FRP C-bars." *Proc., 3rd Int. Symp. on Non-Metallic FRP Reinforcement for Concrete*
845 *Structures (FRPRCS-3)*, JCI ed., Sapporo, 357-364.
846 Toumpanaki, E., Lees, J.M. and Terrasi, G.P. (2014). "Measurement of the sand coating layer
847 in CFRP tendons through image processing." *Proc.,* 7th International Conference on Fiber
848 Reinforced Polymer (FRP) Composites in Civil Engineering, Vancouver.
849 Toumpanaki, E. (2015). "Durability and bond performance of CFRP tendons in high strength
850 concrete." PhD thesis, University of Cambridge, UK.
851 Verbeck, G.J., and Helmuth, R.A. (1968). "Structures and physical properties of cement
852 paste." *Proc. 5th Int. Symp. on the Chemistry of Cement*, Tokyo, Vol. 3, 1-32.
853 Ward, K. (2009). "How to Determine 50+ Year Behaviour in 3 Terms or Less." 4th year
854 project. University of Cambridge.
855 Zhou, J., Chen, X., and Chen, S. (2012). "Effect of different environments on bond strength
856 of glass fiber-reinforced polymer and steel reinforcing bars." *KSCE J. Civ. Eng.*, 16(6), 994–
857 1002.
858
859
860
861
862

863 **Figures**

864 **Fig. 1:** (a) Shear lag effect (after Achillides and Pilakoutas 2004) and (b) Effect of diameter
865 on the average bond strength.

866 **Fig. 2:** Effect of exposure conditions on bond performance (a) 23°C and (b) 60°C.

867 **Fig. 3:** (a) Schematic illustration of sand coating coverage in HS, FS and UN tendons, outer
868 surface in (b) sand-coated tendon and (c) uncoated tendon.

869 **Fig. 4:** Pull-out test set up (a) Drawing and (b) Photo of actual pull out test.

870 **Fig. 5:** (a) Uncoated bare surface, (b) Uncoated rough resin layer, (c) Sand coated area, (d)
871 Sand coated area - agglomerated sand particles, (e) Microscope image of sand-coated tendon
872 cross-section and (f) Bonded region of a sand-coated tendon.

873 **Fig. 6:** (a) RGB image, (b) Grayscale image, (c) Cropped image, (d) pixel size of sand
874 particles, (e) morphological opening method and (f) Enhanced contrast.

875 **Fig. 7:** Typical experimental pull-out load versus slip plots (a) Abrupt and (b) Smooth.

876 **Fig. 8:** Typical bond failure in (a) Sand-coated tendons and (b) Uncoated tendons.

877 **Fig. 9:** Radial cracking in (a) C-SL-I-FS-23-16, (b) C-SL-I-FS-40-71, (c) D-II-FS-40-35 and
878 (d) C-UN-I-UN-40-16 specimens.

879 **Fig. 10:** Bond strength with equivalent immersion time at 23°C for the (a) C-SL-I-FS, C-SL-
880 I-HS and C-UN-I-UN tendons and (b) D-II-FS tendons.

881 **Fig. 11:** Residual bond strength with equivalent immersion time at 23°C for the C-SL-I-FS,
882 C-SL-I-HS and D-II-FS tendons.

883 **Fig. 12:** Indicative ascending branches of bond stress versus s_1-s_f behaviour at equivalent
884 23°C immersion times for (a) C-SL-I-FS and (b) D-II-FS tendons.

885 **Fig. 13:** *Run*, *Rresin* and *Rsand* ratios for C-SL-I-FS and C-SL-I-HS tendons.

886 **Fig. 14:** (a) Bond strength values versus ratio of sand coating layer for C-SL-I-FS and C-SL-
887 I-HS tendons and (b) bond strength values versus ratio of sand coating layer for D-II-FS.

888 **Fig. 15:** Experimental data versus bond stress slip models.

889

890

891

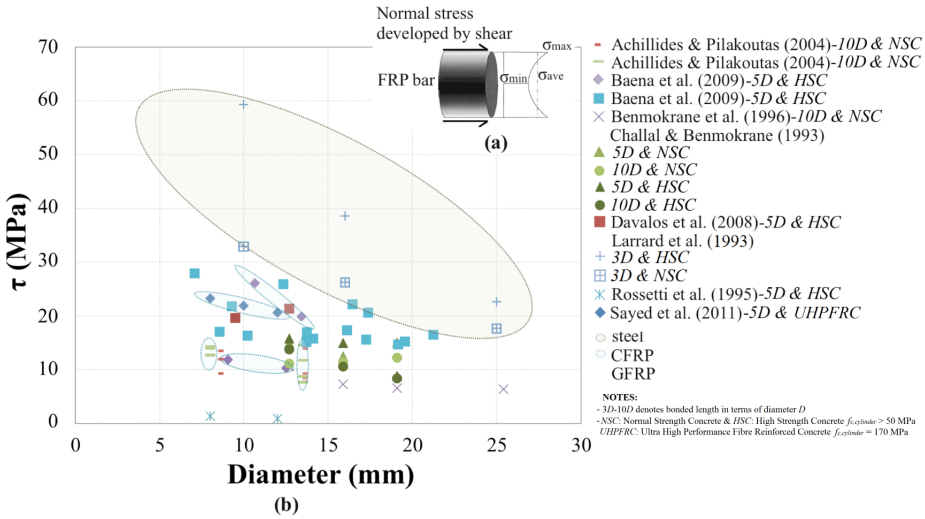

Figure 1

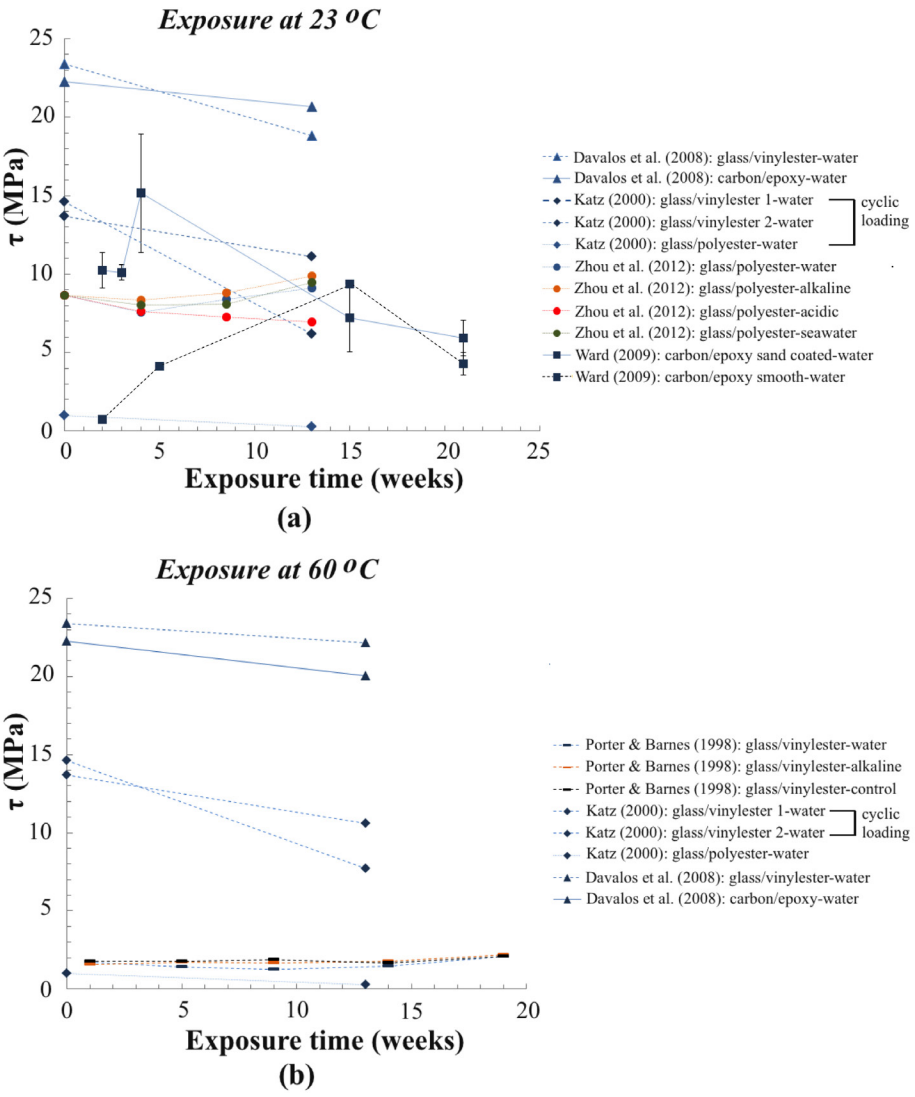

Figure 2

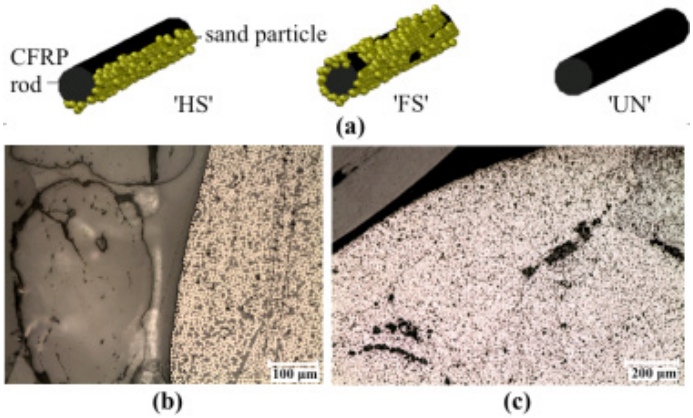

Figure 3

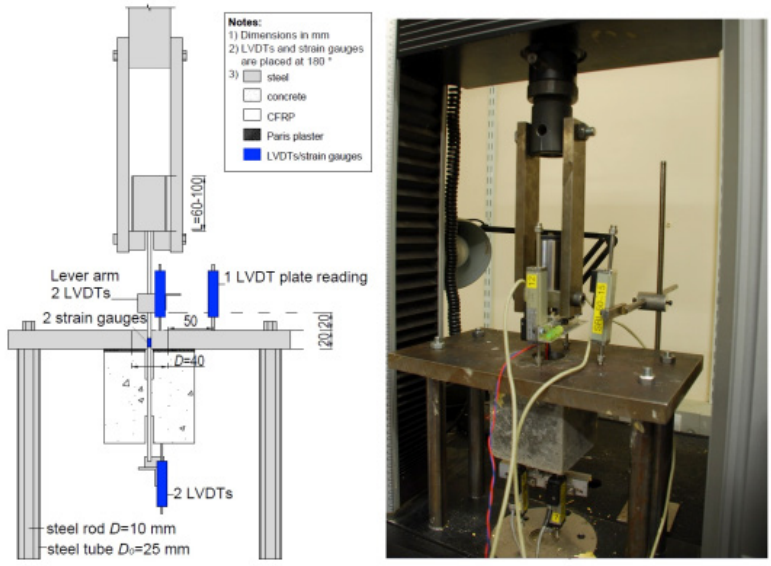

Figure 4

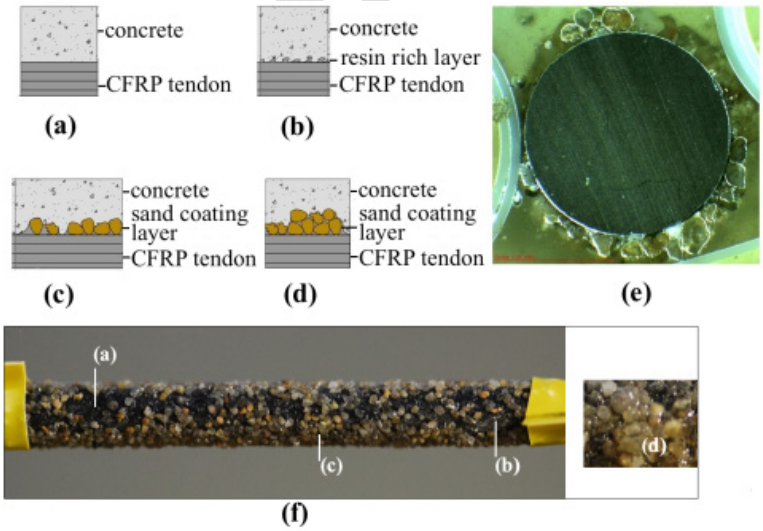

Figure 5

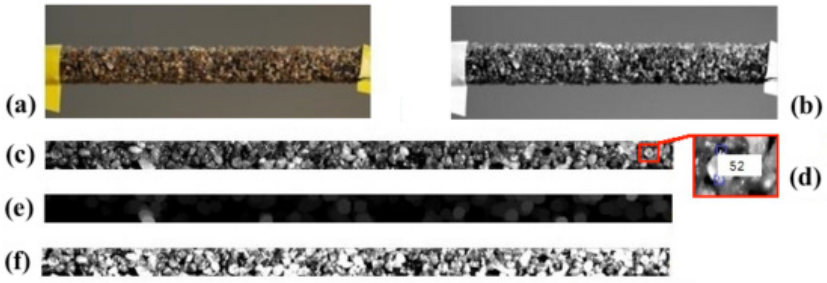

Figure 6

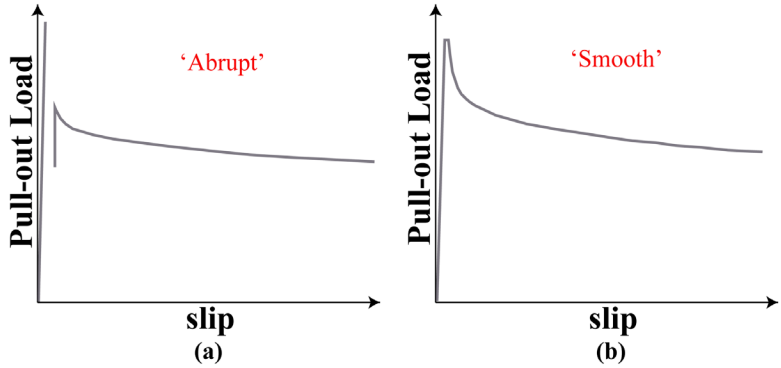

Figure 7

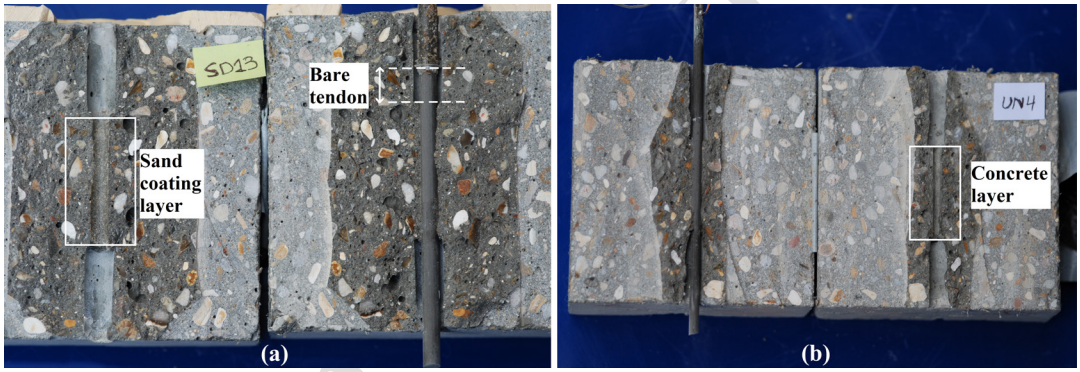

Figure 8

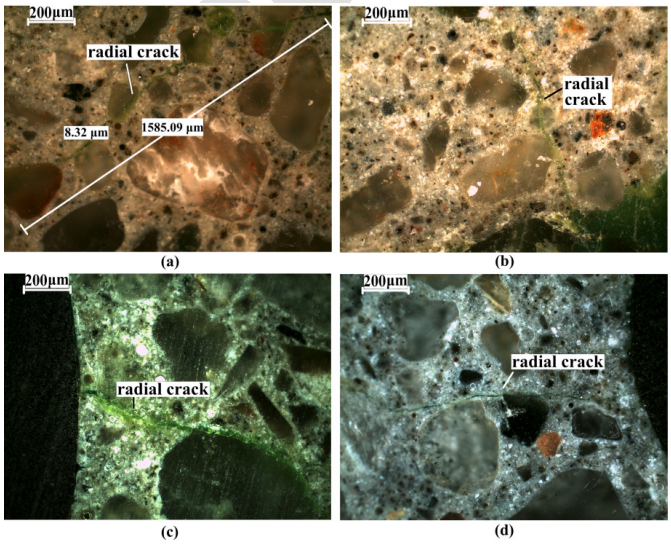

Figure 9

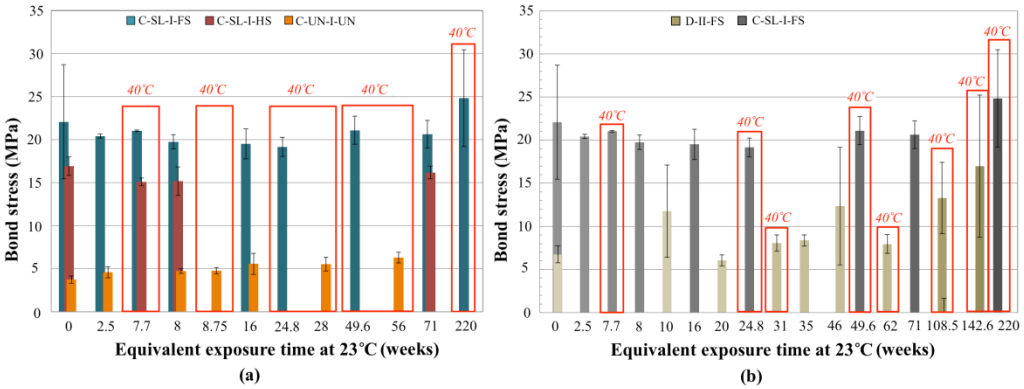

Figure 10

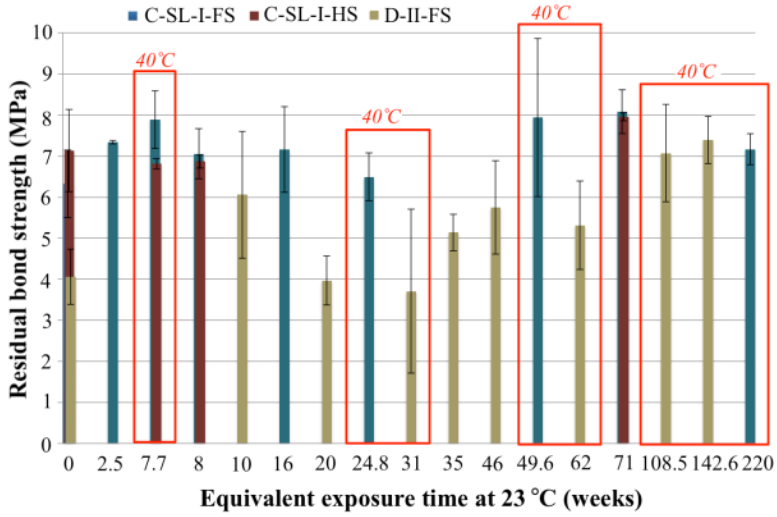

Figure 11

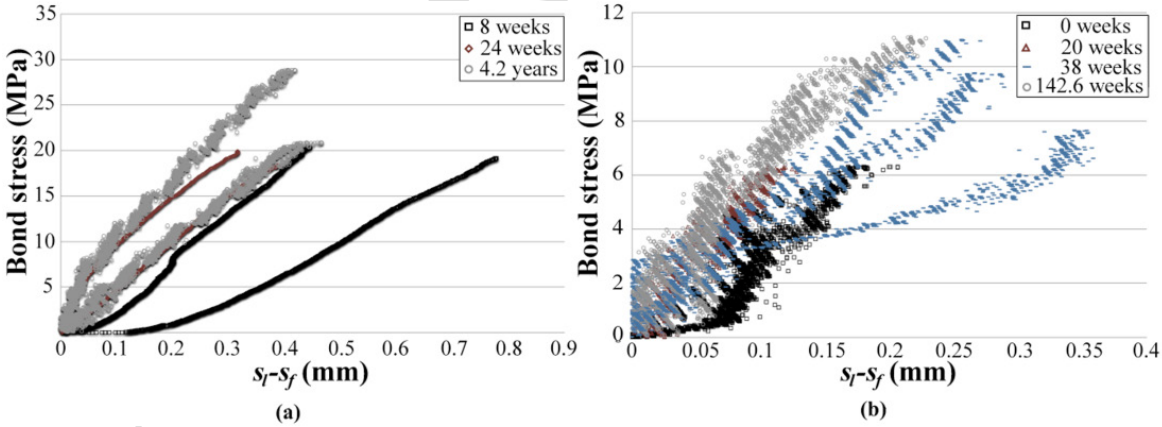

Figure 12

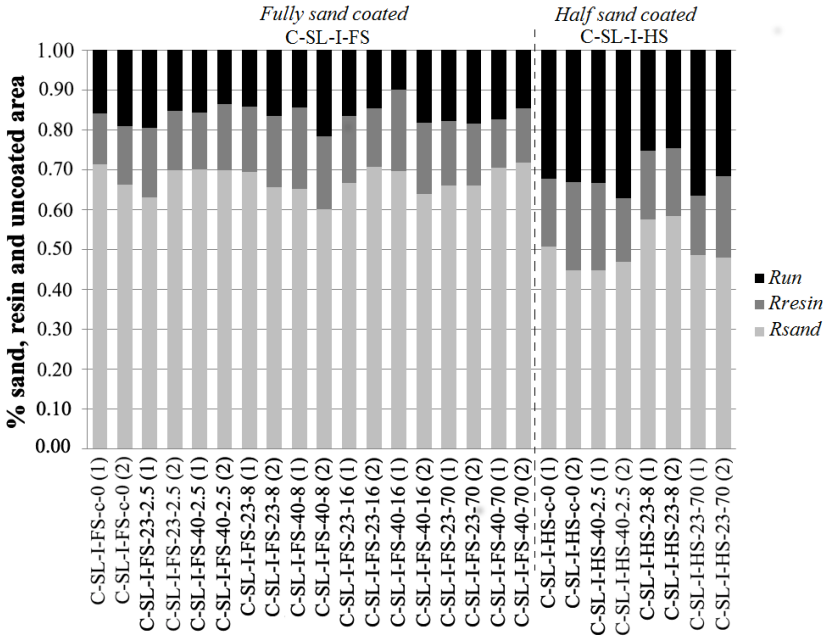

Figure 13

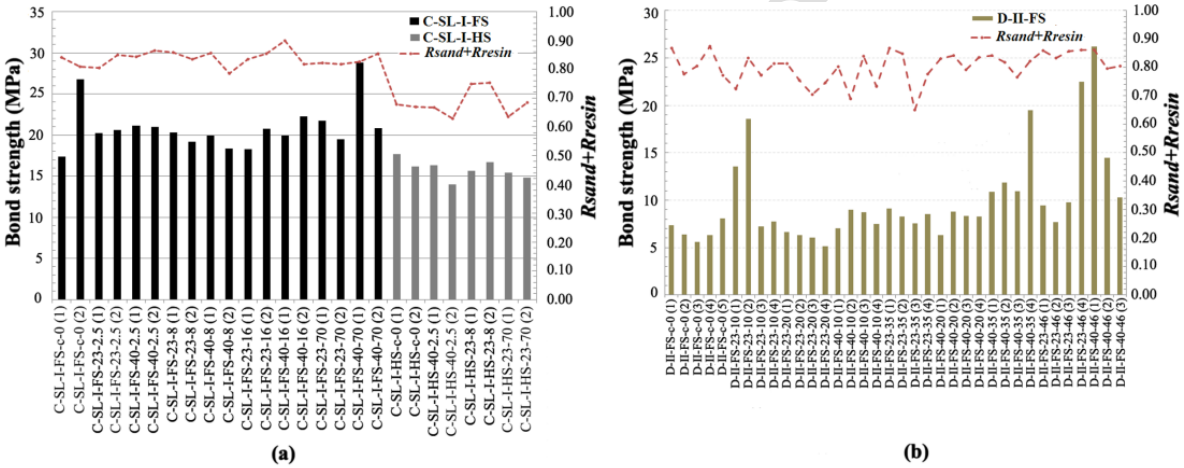

Figure 14

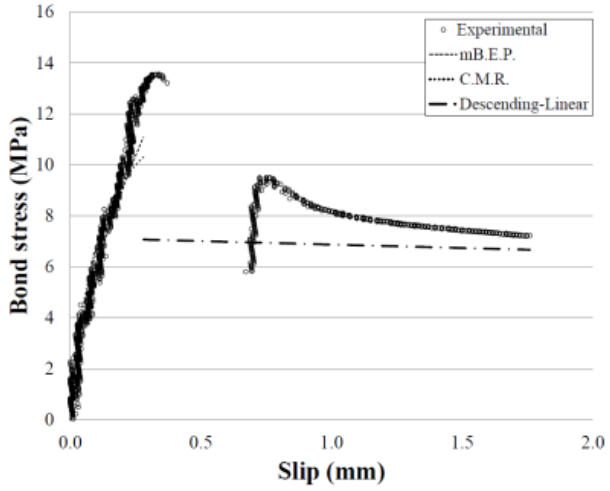

Figure 15

Table 1: Material properties of CFRP tendon specimen

	C-UN	C-SL	D
Matrix/Epoxy hardener	EPR 4434/EPH 943	Rutapox 4539/No data	EPR 4434/EPH 943
Fibres	Tenax UTS 5631	Tenax UTS 5131	Tenax UTS 5631
Nominal core tendon diameter [1] (mm)	4.2	4.2	5.4
Quartz sand coating-Grain size (mm)	-	0.4-0.63	0.4-0.63
Volume fraction	0.64	0.63	0.64
Ultimate tensile strength-average (MPa)	1913	2733	1913
Longitudinal elastic modulus –E_L (GPa)	No data	163	155.7
Initial condition	Uncoated	Originally sand coated	Originally sand coated

Note: [1] The core tendon diameter is the diameter without the sand coating layer (resin rich layer and sand particles).

11 **Table 2:** Concrete properties: mix I and mix II.

12

		Concrete Mix I	Concrete Mix II
w/c		0.3	0.31
Plasticiser	**Type**	Glenium C315	Glenium SKY
	Amount	7.53 lt/m^3	13.59 lt/m^3
Slump flow		520 mm	350-360 mm
Vibration		No	Yes
Initial curing		Immersion in a water bath at 23°C (7 days)	Air curing by sealing with plastic sheeting at 19.7 ± 1.1°C and *RH*= 52 ± 6.7% (14 days)
f_{cu} **(7 day)-cube strength**		55.9 ± 2.6 MPa	75.4 ± 1.1 MPa
CFRP tendons		C-SL, C-UN	D-S

Table 3: Exposure programme for pull-out tests.

Specimen	Exposure	Temperature (°C)	Exposure time (weeks) 0	2.5	8	10	16	20	35	46	71
Full sand-coated tendons											
C-SL-I-FS-c-0	control	wet cure	×(2)								
C-SL-I-FS-23-e	water	23		×(2)	×(2)		×(2)				×(2)
C-SL-I-FS-40-e	water	40		×(2)	×(2)		×(2)				×(2)
D-II-FS-c-0	control	air cure	×(5)								
D-II-FS-23-e	water	23				×(4)		×(4)	×(4)	×(4)	
D-II-FS-40-e	water	40				×(4)		×(4)	×(4)	×(4)	
Half sand-coated tendons											
C-SL-I-HS-c-0	control	wet cure	×(2)								
C-SL-I-HS-40-e	water	40		×(2)							
C-SL-I-HS-23-e	water	23			×(2)						×(2)
Uncoated tendons											
C-UN-I-UN-c-0	control	wet cure	×(4)								
C-UN-I-UN-23-e	water	23		×(2)	×(2)		×(2)				
C-UN-I-UN-40-e	water	40		×(2)	×(2)		×(2)				

Note: × (A): A denotes the number of tested specimens, e= exposure time in weeks.

Table 4: Pull out test results.

Specimen	Exposure time (weeks)	Bond strength τ (MPa)	Concrete strength f_{cu} (MPa)	Longitudinal elastic modulus E_L (GPa)	Loaded end slip value at failure s_l (mm)	Free end slip value at failure s_f (mm)	Pull-out load-slip behaviour
C-SL-I-FS-c-0	control	22.1 (6.63)	55.9	N/A	N/A	N/A	abrupt
C-SL-I-FS-23-2.5	2.5	20.4 (0.25)	87.2	148	N/A	N/A	abrupt
C-SL-I-FS-40-2.5	2.5	21.1 (0.11)	103	151	N/A	N/A	abrupt
C-SL-I-FS-23-8	8	19.8 (0.83)	99.2	161	0.69 (0.24)	0.08 (0.00)	abrupt
C-SL-I-FS-40-8	8	19.2 (1.10)	98.9	151	0.40 (0.03)	0.04 (0.02)	abrupt
C-SL-I-FS-23-16	16	19.5 (1.76)	99.4	145	0.56 (0.34)	0.04 (0.04)	abrupt
C-SL-I-FS-40-16	16	21.1 (1.63)	110	146	0.56 (0.11)	0.04 (0.00)	abrupt
C-SL-I-FS-23-71	71	20.6 (1.59)	106	157	0.38 (0.00)	0.04 (0.01)	abrupt
C-SL-I-FS-40-71	71	24.8 (5.64)	106	148	0.48 (0.01)	0.04 (0.05)	abrupt
D-II-FS-c-0	control	6.8 (0.98)	82.2	142	0.19 (0.11)	0.02 (0.01)	smooth
D-II-FS-23-10	10	11.8 (5.37)	112	145	0.25 (0.11)	0.05 (0.02)	abrupt+smooth
D-II-FS-40-10	10	8.1 (0.95)	111	144	0.16 (0.02)	0.04 (0.01)	abrupt+smooth
D-II-FS-23-20	20	6.1 (0.63)	110	142	0.07 (0.06)	0.01 (0.00)	abrupt
D-II-FS-40-20	20	7.9 (1.09)	106	141	0.12 (0.03)	0.02 (0.01)	abrupt
D-II-FS-23-35	35	8.4 (0.65)	115	142	0.16 (0.07)	0.02 (0.01)	abrupt+smooth
D-II-FS-40-35	35	13.3 (4.14)	115	144	0.22 (0.13)	0.02 (0.01)	abrupt
D-II-FS-23-46	46	12.3 (6.81)	108	142	0.35 (0.07)	0.03 (0.02)	abrupt
D-II-FS-40-46	46	17.0 (8.25)	116	146	0.31 (0.18)	0.06 (0.03)	abrupt
C-SL-I-HS-c-0	control	16.9 (1.07)	55.9	150	N/A	N/A	abrupt
C-SL-I-HS-40-2.5	2.5	15.1 (0.45)	103	146	N/A	N/A	abrupt
C-SL-I-HS-23-8	8	15.2 (1.65)	99.2	146	0.74 (0.49)	0.08 (0.06)	abrupt+smooth
C-SL-I-HS-23-71	71	16.2 (0.72)	106	150	0.33 (0.02)	0.03 (0.00)	abrupt
C-UN-I-UN-c-0	control	3.7 (0.44)	64.7	140	0.39 (0.27)	0.12 (0.03)	smooth
C-UN-I-UN-23-2.5	2.5	4.6 (0.64)	87.2	141	N/A	N/A	smooth
C-UN-I-UN-40-2.5	2.5	4.8 (0.36)	103	141	N/A	N/A	smooth
C-UN-I-UN-23-8	8	4.7 (0.28)	99.2	144	0.43 (0.05)	0.23 (0.30)	smooth
C-UN-I-UN-40-8	8	5.5 (0.81)	98.9	139	0.29 (0.04)	0.01 (0.01)	smooth
C-UN-I-UN-23-16	16	5.6 (1.22)	99.4	143	0.29 (0.14)	0.01 (0.00)	smooth
C-UN-I-UN-40-16	16	6.3 (0.63)	110	143	0.39 (0.15)	0.01 (0.00)	smooth

Table 5: Analytical bond stress-slip results.

Specimen	Ascending branch									Linear descending branch		
	mB.E.P.					C.M.R.						
	τ_m (MPa)	s_m (mm)	α	$(\tau_m/s_m)^{\alpha}$	R^2	τ_m (MPa)	s_m (mm)	β	R^2	τ_{fr} (MPa)	p'	R^2
C-SL-I-FS-23-8	20.1	0.75	1.00	30	0.890	19.7	0.55	1.00	0.758	8.5	0.33	0.823
	(2.26)	(0.30)	(0.00)	(15)		(0.83)	(0.28)	(0.00)		(0.32)	(0.05)	
C-SL-I-FS-40-8	24.3	0.50	0.80	43	0.979	19.2	0.20	1.00	0.957	7.6	0.29	0.725
	(0.24)	(0.09)	(0.13)	(2)		(1.10)	(0.06)	(0.00)		(0.39)	(0.03)	
C-SL-I-FS-23-71	24.00	0.45	0.90	49	0.923	20.6	0.22	1.00	0.875	9.5	0.45	0.769
	(1.50)	(0.02)	(0.15)	(4)		(1.59)	(0.06)	(0.00)		(0.13)	(0.05)	
C-SL-I-FS-40-71	23.1	0.40	0.81	48	0.992	24.8	0.23	1.00	0.953	8.6	0.40	0.770
	(0.60)	(0.11)	(0.16)	(4)		(5.64)	(0.03)	(0.00)		(0.21)	(0.02)	
C-SL-I-HS-23-8	15.0	0.86	1.00	26	0.840	15.2	0.73	1.00	0.744	8.1	0.32	0.769
	(1.94)	(0.65)	(0.00)	(22)		(1.65)	(0.73)	(0.00)		(0.31)	(0.02)	
C-UN-I-UN-23-8	3.5	0.41	1.00	9	0.795	4.7	0.43	1.00	0.669	3.2	0.19	0.717
	(0.88)	(0.02)	(0.00)	(2)		(0.28)	(0.14)	(0.00)		(0.21)	(0.06)	
D-II-FS-c-0	9.4	0.32	0.95	30	0.860	6.9	0.14	1.00	0.749	4.4	0.142	0.926
	(3.67)	(0.15)	(0.10)	(7)		(1.67)	(0.03)	(0.16)		(0.74)	(0.02)	
D-II-FS-23-10	11.1	0.28	0.61	28	0.937	11.7	0.15	0.76	0.909	7.1	0.27	0.846
	(3.72)	(0.09)	(0.28)	(17)		(5.26)	(0.06)	(0.34)		(2.10)	(0.15)	
D-II-FS-40-10	7.3	0.14	0.74	32	0.948	8.1	0.08	0.99	0.875	4.1	0.14	0.877
	(1.12)	(0.04)	(0.08)	(4)		(0.95)	(0.01)	(0.01)		(2.00)	(0.01)	
D-II-FS-23-46	10.7	0.38	0.63	23	0.930	12.5	0.32	0.72	0.890	6.3	0.19	0.910
	(5.69)	(0.09)	(0.29)	(17)		(6.74)	(0.15)	(0.33)		(1.38)	(0.09)	
D-II-FS-40-46	13.1	0.23	0.90	48	0.959	17.0	0.18	1.00	0.910	7.9	0.17	0.852
	(6.03)	(0.12)	(0.14)	(9)		(8.24)	(0.11)	(0.00)		(0.88)	(0.10)	

Note: average value (standard deviation).